Infrared Spectra and Density Functional Calculations for Early First-Row Transition Metal Nitrosyls in Solid Neon

Lester Andrews* and Xuefeng Wang

Department of Chemistry, University of Virginia, McCormick Road, P.O. Box 400319, Charlottesville, Virginia 22904-4319

Received: September 10, 2001; In Final Form: November 30, 2001

Reactions of laser-ablated Sc, Ti, V, Cr, and Mn with NO in excess neon give the same major products found in excess argon with several interesting differences. The argon-to-neon matrix shifts range from +43 cm^{-1} for the small $Sc[NO]^+$ cation to −5 cm^{-1} for Sc[NO]. The lower polarizability of neon leads to a slower condensation rate and allows more reagent diffusion and reaction under the conditions of these experiments, and as a result, higher nitrosyls are observed on condensation in excess neon. Another consequence of the slower condensation rate of neon is the inability to trap as much of the side-bound M[NO] precursor relative to the NMO insertion product: higher yields of M[NO] species are trapped in solid argon. An advantage of the greater inertness of neon is its ability to trap cations with less perturbation than argon. Model calculations show that argon interacts more strongly with $Sc[NO]^+$ than with neon: the $ArSc[NO]^+$ species is stable and has a lower N−O stretching frequency than $NeSc[NO]^+$. New CCl_4 doping experiments and DFT calculations confirm the new observation of $V[NO]^+$ and the previous identification of $Cr(NO)_3^-$, which is a stable anion that might be observable in the gas phase.

Introduction

The interaction of nitric oxide with transition metals is important in catalysis and in biochemistry.[1−4] In addition light-induced isomerization of nitrosyl complexes has technical applications for information storage.[5,6] Matrix isolation investigations of the reaction of transition metal atoms with NO in excess argon have characterized three different types of reaction product: the end-bonded nitrosyl MNO, the side-bonded nitrosyl M[NO], and the NMO insertion product.[7−15] Exposure of these samples to irradiation with visible and ultraviolet light induces rearrangements between these isomers. Density functional theory (DFT) calculations provide vibrational frequencies and isotopic displacements of sufficient accuracy to confirm the identifications of new transition metal (TM) nitrosyl species.

Complementary neon matrix investigations have been performed for the early first row metals. Because neon is more inert than argon, solid neon interacts less strongly with guest species and produces frequencies closer to the yet-to-be measured gas phase values particularly for the more strongly interacting cation products. In addition, the slower condensation rate of neon allows less efficient relaxation, which will affect isomerization processes and higher order reactions. The results of neon matrix investigations and new DFT calculations on Sc, Ti, V, Cr, and Mn nitrosyl systems will be presented here.

Experimental and Theoretical Methods

The experiment for laser ablation and matrix isolation has been described in detail previously.[16,17] Briefly, the Nd:YAG laser fundamental (1064 nm, 10 Hz repetition rate with 10 ns pulse width) was focused on rotating metal targets (Johnson−Matthey). Laser energies ranging from 1 to 40 mJ/pulse were used. Laser-ablated metal atoms, cations and electrons were co-deposited with nitric oxide at 0.1 to 0.3% in neon onto 4−5 K CsI window at 2−4 mmol/h for 30 min to 1 h using an old APD Cryogenics Heliplex or a new Sumitomo Heavy Industries Model RDK-205D Cryocooler. Several isotopic samples ($^{14}N^{16}O$, Matheson; $^{15}N^{16}O$, MDS isotopes, 99%; $^{14}NO + {}^{15}NO$; $^{14}N^{16}O + {}^{14}N^{18}O$ prepared by reaction of $^{14}N^{16}O + {}^{18}O_2$ followed by reduction with Hg and fractional distillation under vacuum) were used. Infrared spectra were recorded at 0.5 cm^{-1} resolution on a Nicolet 750 spectrometer with 0.1 cm^{-1} accuracy with a HgCdTe detector. New experiments were also performed with 10% as much CCl_4 as NO to capture electrons, alter the product yield, and provide supporting evidence for cation and anion identifications.[18,19] Matrix samples were annealed at a range of temperatures (6−12 K, neon) and subjected to broadband photolysis by a medium-pressure mercury arc (Philips, 175 W) with the globe removed ($\lambda > 240$ nm).

Additional density functional theory (DFT) calculations were performed on vandium and chromium nitrosyls using the Gaussian 98 program.[20] The BPW91 functional was used in all calculations, and the BP86 functional was employed for comparison in selected cases.[21−23] The 6-311+G* basis set was used to represent nitrogen, and oxygen, and the Wachters−Hay basis set as modified in Gaussian was used for transition metals.[24−26]

Results and Discussion

Laser-ablated early TM experiments with NO in excess neon produce a number of metal independent absorptions due to $(NO)_2$, $(NO)_2^+$, $(NO)_2^-$, $(NO)_3^-$, NO_2, N_2O_3, and NO_2^- species, which have been tabulated and identified previously.[15,27−29] Also included in Table 1 is a strong, sharp 1857.8 cm^{-1} absorption and sharp, weak 1828.7, 1825.8 cm^{-1} and 1819.1, 1816.8 cm^{-1} doublets, which are probably due to various $(NO)_x(NO)$ clusters. Several new metal dependent bands, neon matrix counterparts of early TM nitrosyl species, and supporting DFT calculations will be described. Tables 1−5 present the results for each metal.

10.1021/jp013443d CCC: $22.00
Published on Web 01/29/2002

TABLE 1: Infrared Absorptions (cm^{-1}) from Co-deposition of Laser-Ablated Scandium with NO in Excess Neon

$^{14}N^{16}O$	$^{15}N^{16}O$	$^{14}NO/^{15}NO$[a]	identification
1877.4	1844.4	1.0179	NO site
1874.4	1841.4	1.0179	NO
1866.3	1833.4	1.0179	*cis*-$(NO)_2$
1860.9	1827.8	1.0181	$(NO)_x(NO)$
1857.8	1824.9	1.0180	$(NO)_x(NO)$
1828.7	1794.8	1.0188	$(NO)_x(NO)$
1825.8	1791.9	1.0189	$(NO)_x(NO)$
1819.1	1785.2	1.0190	$(NO)_x(NO)$
1816.8	1782.9	1.0190	$(NO)_x(NO)$
1780.4	1748.8	1.0181	*cis*-$(NO)_2$
1778.8	1747.4	1.0180	*cis*-$(NO)_2$ site
1762.4	1731.6	1.0178	*trans*-$(NO)_2$
1760.5	1729.9	1.0177	*trans*-$(NO)_2$
1718.5	1688.4	1.0178	phot pdt
1709.6	1677.8	1.0185	aggregate
1673.9	1643.3	1.0186	$Sc(NO)_2$
1658.2	1629.4	1.0177	X-NO
1619.0	1591.1[c]	1.0175	$(NO)_2^+$
1589.4	1559.4	1.0194	ScNO
1572.9	1543.6[b]	1.0190	$Sc(NO)_2$
1511.2	1483.2	1.0189	aggregate
1424.1	1399.3[c]	1.0177	$(NO)_2^+$
1369.9	1346.4[c]	1.0175	$(NO)_3^-$
1188.5	1176.9	1.0099	aggregate
1159.8	1143.0	1.0147	$Sc[NO]^+$
1061.0	1042.3	1.0179	$N_2O_2^{2-}$
1052.6	1034.2	1.0178	$N_2O_2^{2-}$
1006.1	1006.1	1.0000	ScO^+
1001.9	973.6[c]	1.0291	$(NO)_3^-$
962.0	962.0	1.0000	ScO
931.1	931.3	1.00	NScO
928.4	928.4	1.0000	NScO site
861.8	850.2	1.0136	Sc[NO] site
860.8	849.3	1.0137	Sc[NO]
693.8	674.5[c]	1.0286	$(NO)_3^-$
654.2	653.2	1.0015	aggregate
644.4	633.4	1.0174	Sc[NO]
642.6	632.3	1.0163	Sc[NO] site
480.8	468.7	1.0258	NScO
474.6	463.1	1.0248	NScO site

[a] Isotopic frequency ratio. [b] New intermediate component observed at 1556.3 cm^{-1} in $^4NO + ^{15}NO$ experiment. [c] References 28 and 29.

TABLE 2: Infrared Absorptions (cm^{-1}) from Co-deposition of Laser-Ablated Titanium with NO in Excess Neon

$^{14}N^{16}O$	$^{15}N^{16}O$	$^{14}NO/^{15}NO$[a]	identification
1477.6	1441.5	1.0250	$OTi(N_2)O$
1476.0	1439.9	1.0251	$OTi(N_2)O$
1369.9	1346.4	1.0175	$(NO)_3^-$
1159.3	1137.4	1.0193	aggregate
1142.0	1124.5	1.0156	-?-
1126.2	1107.8	1.0166	-?-
1061.0	1042.3[b]	1.0179	$N_2O_2^{2-}$
1052.6	1034.4[b]	1.0178	$N_2O_2^{2-}$
1001.9	973.6	1.0291	$(NO)_3^-$
997.6	997.6[c]		TiO
989.6	989.6		$OTi(N_2)O$
962.7	962.7[c]		TiO_2
955.1	955.1		$TiO_2(NO)_x$
936.5	936.5[c]		TiO_2
925.3	925.3		$TiO_2(NO)_x$
915.0	912.5	1.0027	NTiO
889.0	889.0		$TiO_2(NO)_x$
791.4	789.0	1.0030	$(NTiO^-)$
732.0	714.9	1.0239	NTiO
719.2	705.1	1.0200	NTiO(NO)
693.9	675.6	1.0286	$(NO)_3^-$

[a] Isotopic frequency ratio. [b] See ref 32. [c] See ref 31.

Scandium. Laser-ablated scandium reacts with NO in excess neon to give NScO as the major product (Figure 1). The NScO stretching modes in solid neon, 931.1 and 480.8 cm^{-1} are blue shifted 21.6 and 9.7 cm^{-1} or 2.4 and 2.1%, respectively, from the argon matrix observations.[12] The 931.1 cm^{-1} absorption reveals a 931.1−892.3 cm^{-1} doublet with $N^{16}O + N^{18}O$ and almost the same oxygen isotopic shift found in solid argon. The 480.8 cm^{-1} band exhibits a 480.8−468.7 cm^{-1} doublet with $^{14}NO + ^{15}NO$ and almost the same nitrogen isotopic shift observed in solid argon. The 931.1 cm^{-1} band is 0.7 cm^{-1} wide at half-maximum, and the ^{15}NO counterpart measures 931.3 cm^{-1} although a 0.1 cm^{-1} red shift was calculated. Both of these bands are probably 931.2 ± 0.1 cm^{-1}. The weak 962.0 cm^{-1} band is due to ScO in solid neon based on our argon matrix work.[30]

The other two primary products ScNO and Sc[NO] are observed at 1589.4 cm^{-1} and at 860.8, 644.4 cm^{-1} in solid neon. The 1589.4 cm^{-1} band increases on 9 K annealing, decreases on photolysis, increases on 11 K and decreases on 12 K annealing, and the 860.8, 644.4 cm^{-1} bands increase slightly on annealing, and decrease markedly on photolysis while NScO increases, as observed in solid argon. Note that ScNO is blue shifted 26.1 cm^{-1} in neon, whereas Sc[NO] is red shifted 4.5 and 1.5 cm^{-1}.

The new 1589.4 cm^{-1} ScNO band exhibited 1589.4−1559.4 cm^{-1} and 1589.4−1553.1 cm^{-1} doublets in mixed isotopic experiments with 14/15 isotopic frequency ratio 1.0194 and 16/18 ratio 1.0234; virtually the same ratios were determined for the argon matrix frequencies. The 860.8 cm^{-1} band gave doublets at 860.8−849.3 cm^{-1} and 860.8−844.9 cm^{-1} with 14/15 isotopic ratio 1.0135 and 16/18 ratio 1.0188 which are slightly smaller than the 1.0142 and 1.0209 ratios for the 865.5 cm^{-1} argon counterpart.

The 1159.8 cm^{-1} band increases slightly on photolysis and sharpens on further annealing. This band shows a 1143.0 cm^{-1} ^{15}NO counterpart and a sharp pure isotopic doublet with mixed $^{14}NO+^{15}NO$. The ^{15}NO shift, 16.8 cm^{-1}, is exactly the same observed for the 1117.0 cm^{-1} band assigned to $Sc[NO]^+$ in solid argon. The low 14/15 isotopic frequency ratio, 1.0147, is characteristic of the side-bound species with different mode mixing from the end-bound species, which has a high 14/15 ratio, 1.0194, compared to NO itself, 1.0179. The 1159.8 cm^{-1} band yield was doubled relative to the 861.8 cm^{-1} band on the addition of CCl_4. The 1159.8 cm^{-1} absorption is just above the BP86 (1146.9 cm^{-1}) and B3LYP (1158.2 cm^{-1}) computed N−O stretching fundamental for $Sc[NO]^+$ and is assigned to this primary cation reaction product. Finally, the observation of the side-bound cation isomer is in agreement with early DFT predictions.[33]

It is interesting to note that $Sc[NO]^+$ is blue shifted by a larger amount, 42.8 cm^{-1} or 3.8%, from solid argon to neon, than any of the species observed here including ScO^+ at 1006.1 cm^{-1} with a 29.8 cm^{-1} blue shift. The 1006.1 cm^{-1} band is favored relative to ScO at 962.0 cm^{-1} (7.2 cm^{-1} blue shift) with CCl_4 added, and is observed in O_2 experiments with a 964.2 cm^{-1} $Sc^{18}O^+$ counterpart. Clearly, the cations with ion-induced dipole interactions can interact more strongly with the argon matrix host than the neutral molecules, and cation argon-to-neon matrix shifts will be larger.

New calculations were performed for $Sc[NO]^+$ and the $NeSc[NO]^+$ and $ArSc[NO]^+$ complexes as model systems for the matrix, and the results are listed in Table 6. The new BPW91 results for $Sc[NO]^+$ are virtually the same as reported using the BP86 functional. Note that the strong N−O stretching frequency calculated for $Sc[NO]^+$ at 1146.7 cm^{-1} red shifts to 1139.1 cm^{-1} for $ArSc[NO]^+$ and blue-shifts to 1147.0 cm^{-1}

TABLE 3: Infrared Absorptions (cm^{-1}) from Co-deposition of Laser-Ablated Vanadium with NO in Excess Neon

$^{14}N^{16}O$	$^{15}N^{16}O$	$^{14}N^{18}O$	$^{14}N^{16}O + {}^{15}N^{16}O$	$^{14}NO/{}^{15}NO$[a]	$N^{16}O/N^{18}O$[a]	identification
1874.4	1841.4	1825.7		1.0179	1.0267	NO
1866.4	1833.6	1818.1	1852.4[a]	1.0179	1.0266	$(NO)_2$
1780.4	1748.8	1734.4	1761.8[a]	1.0181	1.0265	*cis*-$(NO)_2$
1778.8	1747.4	1732.9	1760.1[a]	1.0180	1.0265	*cis*-$(NO)_2$ site
1728.7	1696.5			1.0190		$V(NO)_3$ site
1724.0	1691.8			1.0190		$V(NO)_3$
1685.5	1653.9		1676, 1670, 1661	1.0191		$V_x(NO)_y$
1658.3	1629.5		1658.3,1629.5	1.0177		X-NO
1627.8	1598.4	1587.6	1627.8, 1610.8, 1598.4	1.0184	1.0253	$V(NO)_2$
1619.0	1591.1	1577.4	1619.0, 1604.5, 1591.1	1.0175	1.0264	$(NO)_2^+$
1500.8	1465.2		1496.9, 1470.8[b]	1.0243		$OV(N_2)O$
1424.1	1399.4	1388.0				$(NO_2)^+$
1180.3	1150.7			1.0257		$OV(N_2)O$ site
1177.0	1147.3		1166.2, 1157.8[b]	1.0259		$OV(N_2)O$
1146.5	1128.4	1118.8		1.0160	1.0248	$V[NO]^+$
1143.7	1124.9	1115.3	1143.7, 1124.9	1.0167	1.0255	$V[NO]^+$
1069.8	1056.4	1040.9	1069.8, 1056.4	1.0127	1.0278	V[NO]
1052.6	1034.2			1017.8		$N_2O_2^{2-}$
1041.8	1041.8					V_xO_y
1020.5	1012.5			1.0079		NVO^+
1007.0	982.2	1005.1	1007.0, 982.2	1.0252	1.0019	NVO
997.3	997.6	951.4				NVO(NO), VO
974.7	974.7	936.2			1.0411	VO_2 complex
947.2	947.2	(912)	947.2			VO_2
912.0	910.7	875.4	912.0, 910.7	1.0014	1.0418	NVO
909	907					NVO(NO)
766.3	748.3					$OV(N_2)O$

[a] Isotopic frequency ratios. [b] Mixed-isotopic intermediate components.

TABLE 4: Infrared Absorptions (cm^{-1}) from Co-deposition of Laser-Ablated Chromium with NO in Excess Neon

^{14}NO	^{15}NO	$^{14}N^{18}O$	$^{14}NO+{}^{15}NO$	$^{14}NO/{}^{15}NO$	identification
1762.4	1731.6			1.0178	tr-$(NO)_2$
1760.5	1729.9	1715.3		1.0177	tr-$(NO)_2$
1734.5	1701.3	1696.3	1734.9, 1724.5, 1715.7, 1708.0, 1701.3	1.0197	$Cr(NO)_4$
1724.8	1692.0			1.0194	$Cr(NO)_3[NO]$
1711.0	1676.9			1.0203	aggregate
1696.1	1663.7			1.0195	aggregate
1682.6	1650.3			1.0196	$Cr(NO)_3$
1675.4	1643.3	1637.7		1.0195	$Cr(NO)_3$
1637.5	1604.1		1637.5, 1604.1	1.0208	CrNO
1628.8	1597.3		1629.1, 1610.0, 1597.2	1.0199	$Cr(NO)_2$
1619.1	1591.2		1619.1, 1604.5, 1591.2		$(NO)_2^+$
1557.8	1525.9		1557.8, 1544.8, 1533.4, 1525.8		$Cr(NO)_3^-$
1532.2	1495.6		1532.2, 1525.7, 1499.2, 1495.6		aggregate
1519.9	1489.1		not observed	1.0202	$Cr(NO)^-$
1494.1	1468.3		broad doublet on annealing	1.0177	aggregate
1449.7	1424.1		1449.7, 1424.1		$Cr(NO)_3[NO]$
1424.1	1399.5		1424, 1411, 1399.5		$(NO)_2^+$
1194.5	1172.8 sh		1194.5, 1189.4, 1183.5, 1172.8	1.0185	?
1165.6	1145.2 br		1165.4, 1145.2	1.0178	?
1123.9	1105.4		1123.9, 1105.4 sh	1.0167	Cr[NO]
1052.6	1034.2			1.0178	$N_2O_2^{2-}$
981.4	981.4		981.5		aggregate
974.9	974.9[a]		974.9		CrO_2
969.7	944.7	969.2	969.7	1.0265	NCrO
895.8	892.1		895.8, 892.1	1.0041	complex
869.1	868.9	833.3	869.0	1.0002	NCrO
867.1	866.8			1.0003	NCrO(NO)

[a] Zhou, M. F.; Andrews, L. *J. Chem. Phys.* **1999**, *111*, 4230.

for $NeSc[NO]^+$. The calculated $NeSc[NO]^+$-$ArSc[NO]^+$ difference, 7.9 cm^{-1}, is far short of the 42.8 cm^{-1} observed difference, and of course, a larger number of matrix atoms are involved, but such calculations with two and three noble gas atoms failed to converge in a reasonable amount of time. Nevertheless, these calculations predict the correct trend and suggest that the neon−argon matrix difference also approximates the gas-to-argon matrix frequency shift. Computed binding energies for $NeSc[NO]^+$ and $ArSc[NO]^+$ are 1.4 and 5.1 kcal/mol, respectively. Similar calculations for NScO gave the same trend with smaller effects for this weaker interaction.

A new absorption at 1572.9 cm^{-1} exhibits an intermediate component and 1:2:1 intensity pattern with $^{14}NO + {}^{15}NO$ reagent. This is indicative of a vibration involving two equivalent NO subunits. A weaker 1673.9 cm^{-1} band is associated with this absorption. These bands increase slightly on 9 K annealing, decrease about half on photolysis, and increase further on 11 and 12.5 K annealing. Doping with CCl_4 has no effect on these bands. The 1572.9 and 1673.9 cm^{-1} band set is in good agreement with calculated 1546 and 1654 cm^{-1} N−O stretching modes and 10:4 relative intensity for $Sc(NO)_2$.

Titanium. The major Ti and NO reaction product in neon is NTiO as found in argon; weak TiO and TiO_2 bands are also observed.[12,13,31] The strong fundamental absorptions at 915.0 and 732.0 cm^{-1} (Figure 2) are blue shifted 14.4 and 13.8 cm^{-1} or 1.6 and 1.9% from the argon matrix values. The ^{15}NO shifts, 2.5 and 17.1 cm^{-1}, respectively, are the same ±0.1 cm^{-1} as those found in solid argon. Natural titanium isotopic splittings clearly resolved on the sharper lower-frequency absorption again demonstrate the involvement of a single Ti atom. These bands increase 5 ± 1% on annealing to 8 K, 18 ± 4% on annealing to 9.5 K, 5 ± 1% on annealing to 11 K and decrease 33 ± 1% on annealing to 13 K. Clearly, the insertion reaction Ti+NO → NTiO is spontaneous in solid neon at 8 to 11 K.

Weak bands ($A = 0.0006$) at 1061.0 and 1052.6 cm^{-1} after 30 min deposition decreased slightly on deposition for another 30 min. The ^{15}NO counterparts at 1042.3 and 1034.4 cm^{-1} behaved similarly. These features were observed unshifted from scandium experiments. The sharp, weak 1061.0 and 1052.6 cm^{-1}

TABLE 5: Infrared Absorptions (cm^{-1}) from Co-deposition of Laser-Ablated Manganese with NO in Excess Neon

^{14}NO	^{15}NO	$^{14}NO/^{15}NO$	identification
1874.4	1841.4	1.0179	NO
1866.3	1833.4	1.0179	*cis*-$(NO)_2$
1857.8	1824.9	1.0180	$(NO)_xNO$
1828.7	1794.8	1.0188	$(NO)_x(NO)$
1825.8	1791.9	1.0189	$(NO)_x(NO)$
1780.4	1748.8	1.0181	*cis*-$(NO)_2$
1772.8	1741.3	1.0181	$Mn_x(NO)_y$
1768.9	1737.5	1.0181	$Mn_x(NO)_y$
1762.4	1731.6	1.0178	*trans*-$(NO)_2$
1760.5	1729.9	1.0177	*trans*-$(NO)_2$
1757.2	1722.5	1.0201	$M_x(NO)_y$
1754.5	1719.1	1.0206	MnNO
1736.0	1700.6	1.0208	$Mn(NO)_x[NO]$
1724.5	1690.8	1.0199	$Mn(NO)_3$ site
1722.7	1689.1	1.0199	$Mn(NO)_3$ site
1721.8	1688.2[a]	1.0199	$Mn(NO)_3$
1706.2	1672.0	1.0205	$Mn(NO)_2$
1705.3	1671.0[b]	1.0205	$Mn(NO)_2$ site
1489.0	1462.1[a]	1.0184	$Mn(NO)_x[NO]$
1270.0	1249.0[b]	1.0168	$Mn[NO]_2$
1235.7	1215.0	1.0170	Mn[NO]
1060.9	1042.5	1.0176	$N_2O_2^{2-}$ site
1052.8	1034.3[b]	1.0179	$N_2O_2^{2-}$
998.7	998.7		$MnO_2(NO)_x$
996.7	996.7		$MnO_2(NO)_x$
962.2	962.2[c]		MnO_2 (trace)
927.4	917.2	1.0111	NMnO(NO)
922.6	912.9	1.0106	NMnO
882.1	881.9		$NMnO(NO)_x$
872.7	862.4	1.0119	NMnO
868.6	868.2		aggregate
856.5	856.6		aggregate
831.0	831.0[c]		MnO
818.5	818.5[c]		MnOMn

[a] New intermediate components observed at 1708, 1697 cm^{-1} and 1488.2, 1462.3 cm^{-1} in $^{14}NO + ^{15}NO$ experiment. [b] New intermediate component observed at 1683.7, 1259.4 and 1042.9 cm^{-1} in $^{14}NO + ^{15}NO$ experiment. [c] See Chertihin, G. V.; Andrews, L. *J. Phys. Chem. A* **1997**, *101*, 8547.

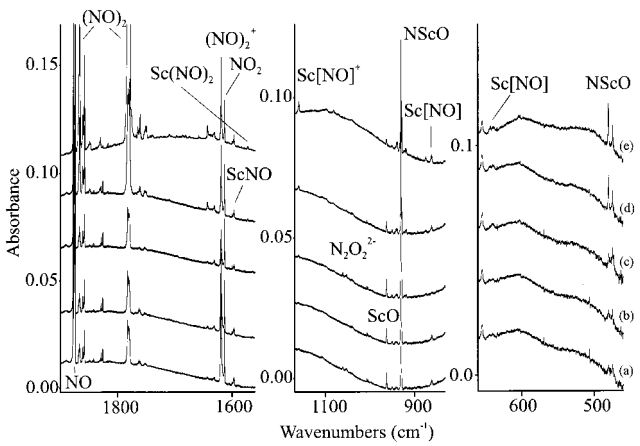

Figure 1. Infrared spectra in the 1900−1560, 1170−830 and 660−460 cm^{-1} regions for laser-ablated Sc co-deposited with 0.2% NO in neon at 4 K: (a) sample deposited for 60 min, spectrum from 64 scans; (b) after $\lambda > 540$ nm photolysis with W lamp; (c) after 240−380 nm photolysis with Hg arc; (d) after 9 K annealing; (e) after 11 K annealing.

absorptions are destroyed by visible but regenerated by ultraviolet light. The isotopic shifts and 1:2:1 triplet pattern with mixed isotopic precursor suggests that these bands are the neon isotopic counterpart of the 1028.5 cm^{-1} argon matrix $N_2O_2^{2-}$ absorption.[32]

Similar experiments were done with zirconium for comparison with the above titanium observations, and the major product

TABLE 6: Parameters Calculated (BPW91/6-311+G*/ Modified Wachters-Hay) for ScNO Species

Sc[NO], $^3A''$, [0.0][a]	1086.8 (140), 614.0 (17), 487.2 (5)[b]
Sc−N: 1.939 Å, Sc−O: 1.939 Å N−O: 1.338 Å	[1068.8, 601.3, 483.9, 1057.2, 611.4, 468.7][c]
NScO, $^3A''$, [4.8][a]	918.3 (188), 459.3 (49), 152.5 (27)
N−Sc: 2.115 Å, Sc−O: 1.689 Å N−Sc−O: 114.1°	
NSc(Ne)O, ^3X, [−0.10][d]	918.5 (189), 459.8 (51), 156.3 (28),
Ne−Sc: 3.132 Å N−Sc: 2.116 Å, Sc−O: 1.689 Å N−Sc−O: 114.2°	47.3 (92), 35.3 (4), 30.1 (1)
NSc(Ar)O, ^3X, [−0.32][d]	915.9 (190), 459.0 (53), 157.5 (32),
Ar−Sc: 3.124 Å N−Sc: 2.117 Å, Sc−O: 1.690 Å N−Sc−O: 114.6°	63.7 (61), 42.2 (8), 35.1 (34)
$Sc[NO]^+$, $^2A''$, [148.0][a]	1146.7 (98), 620.3 (11),
Sc−N: 1.900 Å, Sc−O: 1.911 Å, N−O: 1.317 Å	496.6 (7) [1128.0, 606.8, 493.6, 1115.5, 617.7, 477.9][c]
$NeSc[NO]^+$, ^2X, [−1.4][e]	1147.0 (100), 621.4 (11), 500.5 (6),
Ne−Sc: 2.665 Å Sc−N: 1.901 Å, Sc−O: 1.913 Å N−O: 1.317 Å	91.9 (20), 57.0 (5), 13.3 (24)
$ArSc[NO]^+$, ^2X, [−5.1][e]	1139.1 (105), 623.8 (12), 501.7 (6),
Ar−Sc: 2.788 Å Sc−N: 1.903 Å, Sc−O: 1.915 Å N−O: 1.320 Å	136.9 (40), 85.5 (3), 35.8 (20) [1120.6, 610.2, 498.6, 1107.9, 621.1, 482.8][c]

[a] Relative energy, kcal/mol. [b] Frequencies, cm^{-1} (intensities, km/mol). [c] Frequencies for $^{15}N^{16}O$ and $^{14}N^{18}O$ species. [d] Energies relative to NScO and Ne or Ar. [e] Energies relative to $Sc[NO]^+$ and Ne or Ar.

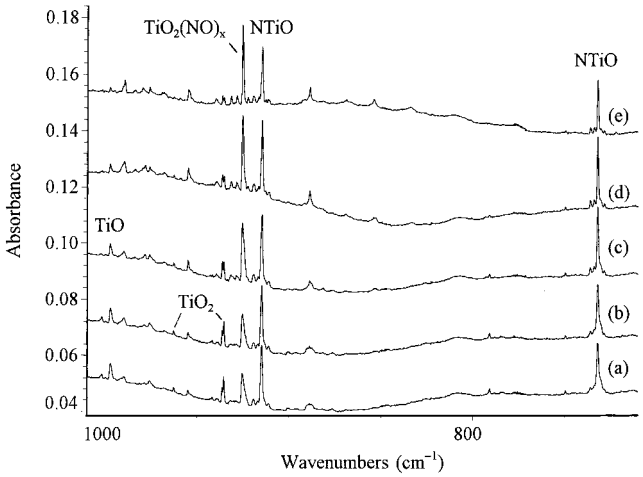

Figure 2. Infrared spectra in the 1010−710 cm^{-1} region for laser-ablated Ti co-deposited with 0.3% NO in neon at 5 K: (a) sample deposited for 60 min; (b) after annealing to 8 K; (c) after annealing to 9.5 K; (d) after annealing to 11 K; (e) after annealing to 13 K.

is again NZrO as found in argon.[34] The fundamental absorptions at 861.3 and 687.9 cm^{-1} are blue shifted 17.1 and 14.6 cm^{-1} or 2.0 and 2.2% from the argon matrix values. The ^{15}NO shifts, 2.8 and 17.9 cm^{-1}, respectively, are the same ± 0.2 cm^{-1} as those found in solid argon. Although interaction with the argon matrix is stronger than interaction with the neon matrix, the normal modes (mostly M═N and M═O stretching modes) are

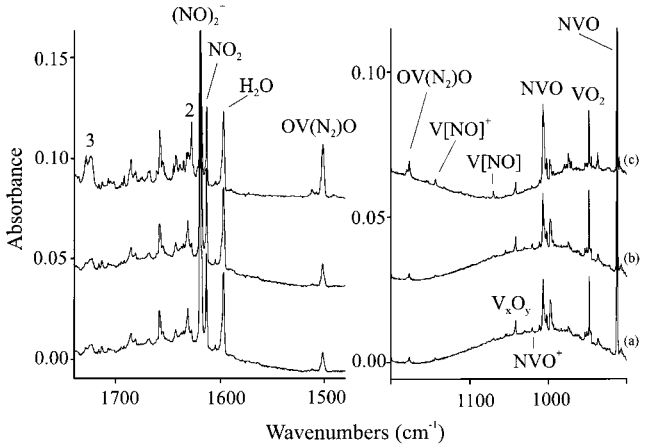

Figure 3. Infrared spectra in the 1750−1480 and 1200−900 cm^{-1} regions for laser-ablated V co-deposited with 0.3% NO in neon at 5 K: (a) sample deposited for 60 min; (b) after annealing to 8 K; (c) after annealing to 11 K.

not changed as measured by isotopic shifts. Annealing to 10 K interchanges matrix site absorptions at 859.3 and 861.3 cm^{-1} and at 685.8 and 687.9 cm^{-1} without increasing the net absorption.

Vanadium. The reaction of laser-ablated V atoms with NO in excess neon is dominated by the NVO insertion product as found for argon matrix reactions.[14] The matrix site structure for complexes with NVO is clearer in solid neon and sharp bands at 1007.0 and 912.0 cm^{-1} are due to NVO in solid neon, blue shifted 8.9 and 5.6 cm^{-1} or 0.9 and 0.6%, respectively, from the argon matrix frequencies. Satellite features at 909.0 and 997.6 cm^{-1} and an underlying band near 1006.5 cm^{-1} are due to NVO complexes with NO (Figure 3).

One disadvantage with solid neon is that temperature excursions for diffusion and further reaction of NO are limited to about 12 K. Nevertheless, the 1007.0 and 912.0 cm^{-1} NVO bands increased 5% in concert: full-arc photolysis had little effect other than to destroy the underlying complex absorption near 1006.5 cm^{-1}. As in solid argon, the NVO bands show isotopic shifts for largely uncoupled V−N and V−O vibrational modes. The NVO bands shift to 982.2 and 910.7 cm^{-1} for ^{15}NV^{16}O and to 1005.1 and 875.4 cm^{-1} for ^{14}NV^{18}O and give a 1.0252 isotopic 14/15 ratio for the upper band, as compared to 1.0272 for VN, and a 1.0418 isotopic 16/18 ratio for the lower band, as compared to 1.0453 for VO. Annealing did increase weak absorptions at 1728.7 and 1627.8 cm^{-1} due to V(NO)$_3$ and V(NO)$_2$, labeled 3 and 2, which are blue shifted 9.1 and 13.3 cm^{-1}, respectively, from argon matrix counterparts.[14]

The 1627.8 cm^{-1} absorption exhibits a 1:2:1 triplet absorption with ^{14}NO + ^{15}NO reagent as expected for V(NO)$_2$. Unfortunately, the strong 1619.1 cm^{-1} (NO)$_2^+$ absorption masks the VNO absorption expected in this region. Annealing increases a 1724.0 cm^{-1} band that is appropriate for V(NO)$_3$. A weak 1075.7 cm^{-1} band in solid argon increased on annealing and exhibited the unusual isotopic frequency shifts for side-bound V[NO]. The neon matrix counterpart is found here at 1069.8 cm^{-1} with similar unusual isotopic frequency ratios (1069.8/1056.4 = 1.0127; 1069.8/1040.9 = 1.0278). This feature increased on annealing as did a weaker band at 1143.7 cm^{-1} (Figure 3) with slightly different frequency ratios (1143.7/1124.9 = 1.0167; 1143.7/1115.3 = 1.0255). A similar experiment with 10% as much CCl_4 as NO increased the relative intensity 1143.7:1069.8 to 3:1 from the 1:2 ratio observed above. Since CCl_4 serves as an electron trap and favors the survival of positive ions, the 1143.7 cm^{-1} band must be considered for V[NO]$^+$.

TABLE 7: Parameters Calculated (BPW91/6-311+G*/Modified Wachters-Hay) for VNO Species

NVO, ^{1}A′, [0.0]^a N−V: 1.569 Å, V−O: 1.631 Å N−V−O: 108.0°	1085.1 (70), 956.0 (213), 423.2 (3)^b [1057.9, 954.9, 416.8; 1083.2, 917.2, 414.1 cm^{-1}]^c
V[NO], ^{3}A″, [+44.3]^a V−N: 1.717 Å, V−O: 1.836 Å N−O: 1.383 Å	1017.3 (149), 643.5 (11), 463.4 (7) [1000.6, 628.9, 460.4; 975.4, 621.6, 445.3 cm^{-1}]^d
NV(Ne)O, ^{1}X, [−0.20]^e Ne−V: 2.663 Å, N−V: 1.570 Å, V−O: 1.632 Å N−V−O: 108.0°	1085.7 (72), 952.5 (211), 423.5 (4), 78.6 (47), 53.5 (5), 39.0 (35)
NV(Ar)O, ^{1}X, [−1.9]^e Ar−V: 2.691 Å N−V: 1.572 Å, V−O: 1.634 Å N−V−O: 108.0°	1082.9 (71), 949.5 (204), 422.2 (3), 136.4 (57), 93.3 (10), 71.5 (22)
NVO$^+$, ^{2}A′, [+205]^a N−V: 1.619 Å, V−O: 1.578 Å N−V−O: 98.8°	1032.9 (37), 812.7 (16), 349.9 (10)^b [1024.9, 797.8, 344.7; 1002.6, 800.5, 342.2 cm^{-1}]^d
V[NO]$^+$, ^{2}A′, [+217]^a V−N: 1.681 Å, V−O: 1.760 Å N−O: 1.376 Å	1077.3 (44), 711.9 (13), 493.7 (3)^b [1060.5, 696.7, 489.7; 1051.3, 700.7, 479.2 cm^{-1}]^c
NeV[NO]$^+$, ^{2}X, [−2.1]^f Ne−V: 2.495 Å N−V: 1.684 Å, V−O: 1.764 Å N−O: 1.374 Å	1080.3 (51), 709.4 (12), 491.5 (3), 117.1 (8), 58.2 (16), 37.5 (22)
ArV[NO]$^+$, ^{2}X, [−8.0]^f Ar−V: 2.604 Å V−N: 1.685 Å, V−O: 1.772 Å N−O: 1.371 Å	1080.6 (62), 706.8 (10), 489.4 (4), 164.8 (22), 77.2 (7), 38.0 (16)
VNO$^+$, $^2\Delta$ [+209] V−N: 1.696 Å, N−O: 1.176 Å	1797.2 (351), 647.5 (0.2), 376.7 (29 × 2)^b [1761.1, 642.4, 367.3; 1757.3, 631.9, 372.0 cm^{-1}]^d
VNO$^+$, $^4\Pi$, [+210] V−N: 1.785 Å, V−O: 1.166 Å	1808.3 (351), 534.3 (2), 296.4 (18 × 2)^b [1768.8, 529.6, 289.1; 1760.1, 522.4, 292.4 cm^{-1}]^d

^{a} Relative energy, kcal/mol. ^{b} Frequencies, cm^{-1} (intensities, km/mol). ^{c} Frequencies for ^{15}N^{16}O and ^{14}N^{18}O species. ^{d} Frequencies for ^{15}N^{16}O and ^{15}N^{18}O species. ^{e} Energies relative to NVO and Ne or Ar. ^{f} Energies relative to V[NO]$^+$ and Ne or Ar.

The results of BPW91 calculations for ^{3}A″ V[NO] and ^{2}A′ V[NO]$^+$ are presented in Table 7. The strong N−O stretching frequencies are predicted at 1017.3 and 1077.3 cm^{-1}; the former may be compared with a 1006.9 cm^{-1} BP86 value and the latter with a 1197.0 cm^{-1} B3LYP result, which are compatible. Our experience is that the pure density functional under-predicts the N−O frequency of side-bound TM-nitrosyls, and the BPW91 computations are 52.5 and 66.4 cm^{-1} too low, respectively. However, the calculated isotopic frequency ratios (1.0167, 1.0258; 1.0158, 1.0247) are in good agreement with observed ratios: this is remarkable in view of the large number of low-lying states for the side-bound species.

The pure density functional finds $^2\Delta$ and $^4\Pi$ VNO$^+$ states 8.1 and 6.9 kcal/mol lower than the ^{2}A′ V[NO]$^+$ structure. This led Zhou and Andrews to assign tentatively a very weak 1720.4 cm^{-1} feature to VNO$^+$ in solid argon.[14] However, CCSD(T) calculations find the ^{2}A′ state to be lower than $^4\Pi$ by 0.6 kcal/mol.[33] Accordingly, the argon matrix experiment was repeated with added CCl_4, and the 1720.4 cm^{-1} band was not enhanced; however, a weak 1139.5, 1137.0 cm^{-1} doublet was enhanced 4-fold relative to the 1078.8, 1075.7 cm^{-1} V[NO] doublet. Hence, an 1139.5, 1137.0 cm^{-1} feature is the argon matrix V[NO]$^+$ counterpart of the 1146.5, 1143.7 cm^{-1} neon matrix bands which were enhanced on deposition with added CCl_4.

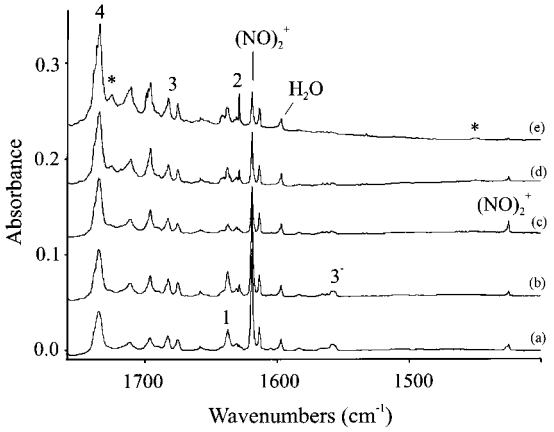

Figure 4. Infrared spectra in the 1750−1400 cm^{-1} region for laser-ablated Cr co-deposited with 0.2% NO in neon at 5 K: (a) sample deposited for 50 min; (b) after annealing to 8 K; (c) after $\lambda > 240$ nm photolysis; (d) after annealing to 10 K; (e) after annealing to 12 K.

The weak 1139.5, 1137.0 cm^{-1} doublet appears in Figure 1c of ref 14 and exhibits a 1119.8 cm^{-1} ^{15}NO counterpart for the stronger 1137.0 cm^{-1} feature. The very weak 1720.4 cm^{-1} band must be attributed to another unidentified nitrosyl complex. Again, the side-bound cation is identified in agreement with early DFT calculations.[33]

Similar calculations were done for Ne and Ar complexes with $V[NO]^+$ and NVO to model the matrix interaction, and the results are given in Table 7. Several comparisons with the analogous scandium species are noteworthy: the Ne and Ar binding energies are slightly stronger and the bonds correspondingly shorter than for the scandium species. The strong N−O stretching frequency is calculated 0.3 cm^{-1} higher for $ArV[NO]^+$ than for $NeV[NO]^+$, which is not the observed trend and suggests that more noble gas atoms need to be considered to properly explain the matrix effect. Likewise for NVO, the very small computed shifts are smaller than observed and point to the need for more noble gas atoms in the calculation, which is beyond our capability.

A weak new absorption is observed at 1020.5 cm^{-1}, which decreases on annealing. The ^{15}NO counterpart at 1012.5 cm^{-1} is enhanced on the addition of CCl_4 to the sample, and only pure isotopic counterparts are observed with $^{14}NO + {}^{15}NO$. This band is in excellent agreement with the strongest band predicted for NVO^+ at 1032.9 cm^{-1}. The computed ^{15}NO shift, 8.0 cm^{-1}, matches the observed shift. Finally, the inserted NVO^+ isomer is the most stable cation arrangement just as NVO is the most stable neutral isomer.

Chromium. The product distribution for laser-ablated Cr with NO in neon is analogous to that found in argon[9] with minor but interesting differences. Figure 4 illustrates spectra in the nitrosyl region on a 5 K optical window. A major band on sample deposition at 1637.5 cm^{-1} (labeled 1) shifts to 1604.1 cm^{-1} with ^{15}NO and reveals a doublet with $^{14}NO + {}^{15}NO$. The 1637.5 cm^{-1} band is assigned to CrNO in solid neon, a 23.2 cm^{-1} blue shift from argon. Annealing produces major growth in a 1628.8 cm^{-1} absorption (labeled 2) that forms a 1:2:1 triplet in the mixed isotopic experiment, which is appropriate for $Cr(NO)_2$ and represents a 5.5 cm^{-1} blue shift from the argon matrix position. Further annealing increases bands at 1682.6 and 1675.4 cm^{-1} (labeled 3) that can be assigned to $Cr(NO)_3$ and the major product at 1734.5 cm^{-1} (labeled 4) to the stable saturated $Cr(NO)_4$ complex. The latter band gave the mixed isotopic pentet for the triply degenerate mode of a tetrahedral species with three weak intermediate components as observed in solid argon. The smaller high-spin CrNO species shows a larger argon-to-neon blue shift (23.2 cm^{-1}) than the larger $Cr(NO)_{2,3,4}$ species (5.5, 12−14, 8.5 cm^{-1}).

A sharp weak 1123.9 cm^{-1} band increases on annealing and decreases on photolysis in favor of sharp NCrO bands at 969.7 and 869.1 cm^{-1}. The 1123.9 cm^{-1} band forms a sharp doublet with both isotopic mixtures, which characterizes a single NO-containing product. The 14/15 and 16/18 ratios, 1.0167 and 1.0263, are appropriate for the side-bound Cr[NO] species found at 1108.8 cm^{-1} in solid argon. The 1165.6 and 1194.5 cm^{-1} neon matrix features clearly involve side-bound NO but their complete stoichiometry cannot be determined.

The $^{14}NCr^{16}O$ absorptions at 969.7 and 869.1 cm^{-1} form sharp doublets with mixed isotopic precursors again confirming that one NO molecule is involved in the reaction. The 969.1 cm^{-1} band shifts to 944.7 cm^{-1} with $^{15}N^{16}O$ giving a 1.0265 ratio, only slightly smaller than the CrN value (1.0273), which demonstrates that the 969.7 cm^{-1} band is essentially a pure Cr−N stretching mode. On the other hand, the 869.1 cm^{-1} band shifts to 833.3 cm^{-1} with $^{14}N^{18}O$ giving a 1.0430 ratio, just smaller than the CrO value (1.0453), which again shows that the 869.1 cm^{-1} band is a largely Cr−O stretching vibration. The 969.7 and 869.1 cm^{-1} bands produced during sample deposition *do not* increase on annealing as do the CrNO and Cr[NO] absorptions; hence, the insertion reaction for Cr requires activation energy. These bands are red shifted 6.4 cm^{-1} (0.7%) and blue shifted 2.9 cm^{-1} (0.3%) by solid neon compared to argon. The growth of NCrO on broadband irradiation at the expense of Cr[NO] strongly suggests the photochemical insertion reaction. The yield of Cr[NO] relative to NCrO absorptions was 5-fold less in solid neon than in argon. Hence, the more strongly interacting argon matrix relaxes the side-bound species faster or increases the potential energy barrier between the two species. We note that BP86 calculations predict a $^4A''$ ground state for Cr[NO] and a $^2A''$ ground state for NCrO so spin change may effectively increase the barrier between Cr[NO] and NCrO, which is the lower energy species by 16.4 kcal/mol. We also note that CrNO ($^4\Sigma^-$) also decreases on photolysis, and this may also contribute to the formation of NCrO.

$$Cr[NO] \xrightarrow{UV-vis} NCrO \qquad (1)$$

Weak bands appear together on late annealing at 1724.8 and 1449.7 cm^{-1} (labeled *) that are due to the $Cr(NO)_3[NO]$ species observed at 1714.2 and 1448.8 cm^{-1} in solid argon from the Cr and NO reaction and from photolysis of $Cr(NO)_4$. The lower frequency absorption is due to NO in a different bonding arrangement, which we believe is side-bound, although DFT calculations failed to locate such a minimum and converged to stable $Cr(NO)_4$.

Bands in solid argon near 1500 cm^{-1} were assigned to $Cr(NO)_n^-$ species and neon matrix counterparts are observed here. The strongest band at 1557.8 cm^{-1} decreases on photolysis and exhibits the mixed isotopic quartet appropriate for the doubly degenerate stretching mode of the trigonal species $Cr(NO)_3^-$. In a neon experiment with CCl_4 added to serve as an electron trap,[18,19] this band was reduced to 10% of the yield without CCl_4, which is diagnostic for an anion absorption as the same effect was found for $(NO)_2^-$. In experiments on a 3.5 K optical window a new sharp 1519.9 cm^{-1} band decreased on annealing and was eliminated with CCl_4: the lack of mixed isotopic bands and proximity to the 1511.5 cm^{-1} argon matrix $CrNO^-$ absorption indicate the same assignment. The weaker $Cr(NO)_2^-$ absorption was not detected in solid neon. The $CrNO^+$ species is predicted to have a $^5\Pi$ ground state with a 1872.0

TABLE 8: Parameters Calculated (BP86/6-311+G*/Modified Wachters-Hay) for Higher Chromium Nitrosyls

$Cr(NO)_3$, $^2A'$, C_s	
2 Cr−N: 1.720 Å; Cr−N′: 1.714 Å	1797.2 (179), 1707.5 (1176), 1695.6 (1371),[a]
2 N−O: 1.185 Å; N′-O: 1.180 Å	698.3 (6), 633.1 (14), 621.7 (4),
2 Cr−N−O: 165.6°; Cr−N′-O: 172.9°	573.5 (2), 512.9 (9)
N−Cr−N: 114.6°; N−Cr−N′: 99.6°	[1760.7, 1673.5, 1662.1; 1720.1, 1633.9, 1622.3 cm^{-1}][b]
$Cr(NO)_3^-$, $^1A_1$, C_{3v}	
Cr−N: 1.706 Å; Cr−N−O: 168.6°	1653.2 (193), 1563.1 (1453 × 2), 716.8 (4),[a]
N−O: 1.218 Å; N−Cr−N: 109.9°	659.9 (3 × 2), 569.2 (2), 553.0 (54 × 2)
	[1618.3, 1530.5; 1583.4, 1497.0][b]
$Cr(NO)_4$, $^1T_2$, T_d	
Cr−N: 1.743 Å[c]	1859.9 (0), 1753.0 (1453 × 3), 705.2 (96 × 3),[a]
N−O: 1.174 Å	526.1 (16 × 3), 496.5 (0), 477.9 (0 × 2),
	321.1 (0 × 3), 73.6 (0 × 3), 64.7 (0 × 2)
	[1718.5, 696.7, 514.5; 1677.1, 690.4, 505.0 cm^{-1}][d]

[a] Frequencies, cm^{-1} (intensities, km/mol), (intensities for degenerate mode × degeneracy). [b] N−O stretching frequencies for $^{15}N^{16}O$ species; for $^{15}N^{18}O$ species. [c] Bond lengths from electron diffraction, 1.763 Å, 1.171 Å, ref 44. [d] The t_2 frequencies for $^{15}N^{16}O$ species; for $^{15}N^{18}O$ species.

TABLE 9: Parameters Calculated (BPW91/6-311+G*/Modified Wachters-Hay) for Chromium Dinitrosyl Species

$Cr(NO)_2$, $^3B_2$, C_{2v}, [0.0][a]	1729.9 (307), 1663.5 (1301), 655.4 (1),[b]
Cr−N: 1.697 Å, N−O: 1.193 Å	600.7 (4), 559.7 (1)
N−Cr−N: 102.2°, Cr−N−O: 169.8°	[1695.1, 1630.1; 1655.6, 1592.0 cm^{-1}][c]
$Cr(NO)_2^-$, $^2A_1$, C_{2v}, [−41.9][a]	1541.3 (405), 1483.9 (1407), 596.3 (25), 576.4 (1)[b]
Cr−N: 1.708 Å, N−O: 1.238 Å	[1508.9, 1453.7; 1476.2, 1420.8 cm^{-1}][c]
N−Cr−N: 125.9°, Cr−N−O: 167.3°	
$Cr(NO)_2^+$, $^2A_1$, C_{2v}, [+176][a]	1923.9 (142), 1835.6 (981)[b]
Cr−N: 1.702 Å, N−O: 1.158 Å	[1885.5, 1799.9; 1841.0, 1755.7 cm^{-1}][c]
N−Cr−N: 90.6°; Cr−N−O: 179.5°	
Cr(NO)[NO], ^3A, C_i, [−43.2]	1695.6 (838), 1244.6 (458), 640.7 (45), 568.8 (36)[b]
Cr−(N): 1.712 Å, (N−O): 1.193 Å	[1661.9, 1222.8; 1622.4, 1190.0 cm^{-1}][c]
Cr-[N]: 1.806 Å, Cr-[O]: 1.943 Å	
[N−O]: 1.278 Å, Cr−(N−O): 170.6°	
(N)-Cr-[N]: 107.0°; (N)-Cr-[O]: 143.2°	
NCrO(NO), ^3A, C_i, [+4.4][a]	1723.6 (613), 1082.6 (67),[b]
N−Cr: 1.549 Å, Cr−O: 1.632 Å	916.7 (144), 745.6 (2), ... 123.9 (15)
N−Cr−O: 110.4°, Cr−(N): 1.878 Å	
(N−O): 1.181 Å; Cr−(N−O): 147.7°	
N−Cr−(N): 107.0°, O−Cr−(N): 112.6°	

[a] Relative energy, kcal/mol. [b] Frequencies, cm^{-1} (intensities, km/mol). [c] N−O stretching frequencies for $^{15}N^{16}O$ species; for $^{15}N^{18}O$ species.

cm^{-1} fundamental. This region was searched in vain for an appropriate band, but NO monomer absorption probably obscures $CrNO^+$ in these experiments.

Additional DFT calculations were done on the Cr/NO system at the BP86/6-311+G*/modified Wachters−Hay level for comparison with previous work.[9] The same $^3B_2$ $Cr(NO)_2$ state was calculated with a Cr−N−O angle of 169.8°. Calculations for $Cr(NO)_3$ started with C_{3v} symmetry and converged to a C_s complex and $^2A'$ state with two equivalent Cr−N−O linkages (1.720, 1.185 Å) and a third slightly different (1.714, 1.180 Å). All computed frequencies are real, and those above 500 cm^{-1} are listed in Table 8 for three isotopic modifications. The two strongest computed N−O stretching modes are slightly different, and two distinct bands are observed in the infrared spectrum in very good agreement. On the other hand, the $Cr(NO)_3^-$ calculation converged a C_{3v} structure and $^1A_1$ state, which is 61.2 kcal/mol lower than $Cr(NO)_3$ and provides an electron affinity estimate for the latter. The doubly degenerate-frequency calculated at 1563.1 cm^{-1} is in excellent agreement with the 1557.8 cm^{-1} neon matrix fundamental for $Cr(NO)_3^-$. This anion should be observable in the gas phase. The saturated $Cr(NO)_4$ molecule was also calculated to provide a consistent set of vibrational frequencies. Previous computations found a tetrahedral geometry but did not provide frequencies.[35−40] The BP86 frequencies, relative intensities, and isotopic frequency ratios are in excellent agreement for the three observed t_2 modes.[9]

Finally, calculations were done for the three bis isomers $Cr(NO)_2$, Cr(NO)[NO] and NCrO(NO) at the BPW91 level. Comparing the calculations in Table 9 with the BP86 results reported previously[9] shows minor differences. Even though NCrO is the global minimum CrNO species,[9] Cr(NO)[NO] is the minimum energy $Cr(NO)_2$ species.

Manganese. Major product absorptions were observed in the end-bound and side-bound nitrosyl and insertion product nitrosyl regions on sample deposition in excess neon, which allowed more reagent diffusion than on sample deposition in excess argon.[10] Photolysis slightly decreased the nitrosyl product absorptions and slightly increased the insertion product in contrast to solid argon. The major end-bound product absorptions at 1754.5, 1721.8, and 1706.2 cm^{-1} (labeled 1, 3, and 2, respectively) increased on 10 and 11 K annealing and decreased on photolysis (Figure 5). Final annealing to 12 K further increased the 1721.8 cm^{-1} band. These bands shifted with ^{15}-NO and gave slightly different $^{14}NO/^{15}NO$ isotopic frequency ratios 1.0206, 1.0199, and 1.0205, respectively, showing the coupling of N−O stretching with another mode. Similar results were found in a more concentrated (0.3%) NO experiment. In this case, the 1757.2 cm^{-1} feature dominated the 1754.5 cm^{-1} absorption providing evidence that the former is a higher cluster. The $^{14}NO + {}^{15}NO$ experiment gave a 1:2:1 triplet at 1705.3, 1683.7, 1671.0 cm^{-1}, which is appropriate for $Mn(NO)_2$. For comparison, in solid argon, the strong $Mn(NO)_2$ absorption at

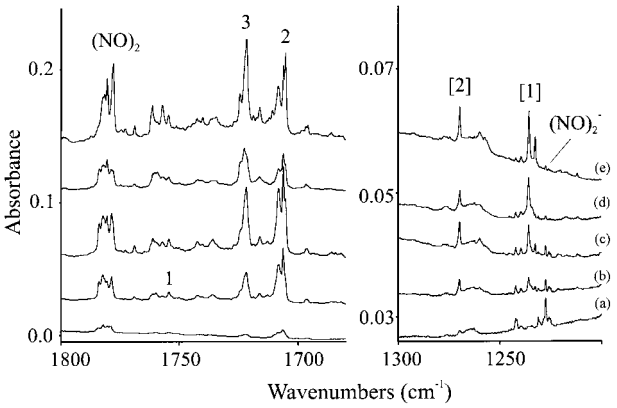

Figure 5. Infrared spectra in the 1800−1680 and 1300−1200 cm^{-1} regions for laser-ablated Mn co-deposited with 0.1% NO in neon at 5 K: (a) sample deposited for 60 min; (b) after annealing to 10 K; (c) after annealing to 11 K; (d) after $\lambda > 240$ nm photolysis; (e) after annealing to 12 K.

1693.0 cm^{-1} exhibited a 1.0204 isotopic 14/15 ratio.[10] The same mixed isotopic experiment gave weak intermediate components for the strong $Mn(NO)_3$ band at 1721.8 cm^{-1}. In solid argon, the very strong $Mn(NO)_3$ band at 1713.2 cm^{-1} exhibited the same 1.0199 isotopic 14/15 frequency ratio. The sharp 1754.5 cm^{-1} band revealed no intermediate components as expected for MnNO, which was tentatively associated with a weak 1748.6 cm^{-1} argon matrix absorption.[10] The neon matrix spectra gave better resolution of this feature and the same 1.0206 isotopic 14/15 frequency ratio.

The observation of MnNO near 1750 cm^{-1} is in very good agreement with DFT predictions for the $^3\Sigma^-$ state but not for the $^5A''$ state computed a few kcal/mol lower.[10] This observation of $^3\Sigma^-$ as the MnNO ground state suggests that the relative computed energies of these states are in error by a few kcal/mol.

The side-bound region (Figure 5) produced two new features at 1220.0 and 1235.7 cm^{-1} on annealing just as found at 1268.7 and 1236.8 cm^{-1} in solid argon.[10] With mixed isotopic precursor the former produced a 1:2:1 triplet and the latter a 1:1 doublet so these bands are in accord with their earlier assignment to $Mn[NO]_2$ and Mn[NO]. The latter species is not complicated by the extra band found in solid argon and attributed to Fermi resonance. The yield of NMnO was less in neon than in argon, and the product bands (Table 5) were slightly red-shifted in solid neon.

The insertion product region revealed isolated and complexed forms of this moiety. The isolated NMnO species increased at 922.6 and 872.7 cm^{-1} on photolysis. These bands are red shifted 9.7 and 1.3 cm^{-1} on 1.0 and 0.1% from argon to neon. The NMnO molecule is the only insertion product investigated that exhibits strongly mixed stretching modes.[41]

Argon-to-Neon Matrix Shifts. The typical way to determine matrix effects is to compare gas-phase spectra.[42] However, none of the transient products described here has been characterized in the gas phase: the stable $Cr(NO)_4$ molecule has been observed by electron diffraction.[43,44] Accordingly, we use the argon-to-neon shift as a measure of the relative guest−host interaction, and take for granted that the interaction is stronger with the more polarizable argon matrix as the neon matrix absorption is closer to the gas-phase value for most molecules.[42] Our calculations for $Sc[NO]^+$ support this proposition. We therefore suggest the neon-to-argon shift as a model for the gas phase to argon shift.

The argon-to-neon matrix shifts given here cover from +42.8 cm^{-1} (or 3.8%) for $Sc[NO]^+$ to −4.5 cm^{-1} for Sc[NO] and are in the +3 to +14 cm^{-1} range for most of the neutral nitrosyls. An exception is CrNO: this high-spin ($^4\Sigma^-$) molecule shows a 23.2 cm^{-1} (or 1.4%) shift. We expect cations to exhibit the largest shifts as they form relatively stronger ion-induced dipole interactions with argon than with neon. This is certainly the case for $Sc[NO]^+$ and $V[NO]^+$. Although noble gas atoms bind more strongly to the vanadium species, the computed Ne−Ar complex difference is larger for $Sc[NO]^+$ as is the observed matrix shift. The small argon-to-neon *red shifts* for Sc[NO] and V[NO] are unusual and may be due to cavity size mismatches where a tighter fit is observed in solid argon. Interestingly, the highest nitrosyls observed here, $V(NO)_3$, $Cr(NO)_4$, and $Mn(NO)_3$ exhibited 8.9, 8.5 and 8.6 cm^{-1} or 0.5% blue shifts, respectively. These are in the expected range for gas-to-argon shifts,[42] and if we assume a negligible gas-to-neon shift, these high nitrosyls behave normally.

An interesting trend is found for the insertion products NScO, NTiO, NVO, NCrO and NMnO. The argon-to-neon shifts for each stretching mode decrease from large blue shifts (2.4, 2.1%), (1.6, 1.9%), (0.9, 0.6%), (−0.7, 0.3%) to small red shifts (−1.0, −0.1%), respectively. These nitride-oxide molecules are unusual as both nitrogen and oxygen are bound to the same metal center. For N−Sc═O the 931.1 cm^{-1} vibration is primarily an Sc═O stretching mode, and the 480.8 cm^{-1} band a Sc−N mode as only three valence electrons are available. However, for N≡V═O five valence electrons are available, and the 1007.0 cm^{-1} vibration is primarily a V≡N mode with the 912.0 cm^{-1} band a mostly V═O mode. Our model calculations find the same percent Ne−Ar complex frequency shifts for NScO and NVO complexes (about 0.3%), in contrast to the above slightly larger percents. One noble gas atom is clearly inadequate to explain the matrix shifts.

Additional calculations were done for NScO at the same level as employed for NVO to seek explanation for the matrix shifts. These BPW91 computations gave almost the same parameters (Table 6), $\mu = 6.61$ D, charges N(−0.33) Sc(+0.77) O(−0.44) as found for $^3A''$ ground-state NScO.[45] The NVO calculation provided $\mu = 6.00$ D, and charges N(−0.37) V(+0.74) O(−0.37). The slightly larger dipole moment for NScO cannot account for the 3-fold larger argon-to-neon matrix shifts compared to NVO. We suggest that with two fewer valence electrons the bare Sc center can interact more intimately with argon atoms. However, calculations of single Ne and Ar complexes with NScO and NVO reveal a slightly stronger interaction with vanadium and suggest that more noble gas atoms must be included to explain the matrix effect.

Conclusions

Reactions of laser-ablated Sc, Ti, V, Cr, and Mn with NO in excess neon give the same major products found in excess argon with several interesting differences.[9,10,12−14] The argon-to-neon matrix shifts run from +42.8 cm^{-1} for the small $Sc[NO]^+$ cation to −4.5 cm^{-1} for Sc[NO] and are typically in the +3 to +14 range for these neutral guest molecules. The more polarizable $N_2O_2^{2-}$ dianion sustains large +24 and +32 cm^{-1} argon-to-neon matrix shift.[32] Clearly, ions interact more strongly with the argon matrix[42] and produce a larger blue shift in solid neon.

The lower polarizability of neon leads to a slower condensation rate and allows more reagent diffusion and reaction under the conditions of these experiments. In other words, at the same mass flow rate, neon condenses more slowly at 4 K than argon at 10 K, and as a result higher nitrosyls are observed on condensation in excess neon, but these higher nitrosyls can be prepared on diffusion of NO on annealing to 30−40 K in solid

argon. Much less diffusion is observed in solid neon at 10−12 K, which is the effective upper temperature limit for the solid neon experiment. Another consequence of the slower condensation rate of neon is the inability to relax and trap as much of the side-bound M[NO] precursor relative to the NMO insertion product. Higher yields of M[NO] species are trapped in solid argon. Side-bound nitrosyl species that are important for information storage[5,6] have been observed for a number of transition metal atoms.[41]

An advantage of the greater inertness of neon is its ability to trap cations with less perturbation than argon. When gas-phase fundamentals are unavailable, the neon-to-argon shift is a good approximation for gas-to-argon shift. The $Sc[NO]^+$ cation interacts much more strongly with argon than neon as the large 42.8 cm^{-1} argon-to-neon red shift and DFT model calculations for $Sc[NO]^+$, $NeSc[NO]^+$, and $ArSc[NO]^+$ indicate. New experiments with CCl_4 added to serve as an electron trap[18,19] confirm the identifications of cations and anions in these experiments. The stable $Cr(NO)_3^-$ anion documented here (DFT electron affinity 61 kcal/mol) should be observable in the gas phase.

Acknowledgment. We gratefully acknowledge support from NSF Grant No. CHE 00-78836 and computer time from the San Diego Supercomputer Center.

References and Notes

(1) Shelef, M. *Chem. Rev.* **1995**, *95*, 209.
(2) Brown, W. A.; King, D. A. *J. Phys. Chem. B* **2000**, *104*, 2578, and references therein.
(3) Perutz, M. F. *Nature* **1996**, *380*, 205.
(4) Squadrito, G. L.; Pryor, W. A. *Free Radical Bio. Med.* **1998**, *25*, 392, and references therein.
(5) Carducci, M. D.; Pressprich, M. R.; Coppens, P. *J. Am. Chem. Soc.* **1997**, *119*, 2669.
(6) Coppens, P.; Fomitchev, D. V.; Carducci, M. D.; Culp, K. *J. Chem. Soc., Dalton Trans.* **1998**, 865.
(7) Chiarelli, J. A.; Ball, D. W. *J. Phys. Chem.* **1994**, *98*, 12828 (Cu + NO).
(8) Ruschel, G. K.; Nemetz, T. M.; Ball, D. W. *J. Mol. Struct.* **1996**, *384*, 101 (Co, Ni + NO).
(9) Zhou, M. F.; Andrews, L. *J. Phys. Chem. A* **1998**, *102*, 7452 (Cr + NO). The computed Cr−N−O angle is 169.8° (all cis) for $^3B_2$ $Cr(NO)_2$.
(10) Andrews, L.; Zhou, M. F.; Ball, D. W. *J. Phys. Chem. A* **1998**, *102*, 10 041 (Mn, Re+NO). The 1487.1 cm^{-1} band should be 1487.5 cm^{-1} and the upper mixed isotopic component should be 1487.3 cm^{-1}.
(11) Krim, L.; Manceron, L.; Alikhani, M. E. *J. Phys. Chem.* A **1999**, *103*, 2592 (Ni + NO).
(12) Kushto, G. P.; Zhou, M. F.; Andrews, L.; Bauschlicher, C. W., Jr. *J. Phys. Chem. A* **1999**, *103*, 478. (Sc, Ti + NO).
(13) Krim, L.; Prot, C.; Alikhani, E. M.; Manceron, L. *Chem. Phys.* **2000**, *254*, 267 (Ti + NO).
(14) Zhou, M. F.; Andrews, L. *J. Phys. Chem. A* **1999**, *103*, 478. (V + NO).
(15) Zhou, M. F.; Andrews, L. *J. Phys. Chem. A* **2000**, *104*, 3915 (Fe, Co, Ni + NO).
(16) Burkholder, T. R.; Andrews, L. *J. Chem. Phys.* **1991**, *95*, 8697.
(17) Hassanzadeh, P.; Andrews, L. *J. Phys. Chem.* **1992**, *96*, 9177.
(18) Zhou, M. F.; Andrews, L. *J. Am. Chem. Soc.* **1998**, *120*, 11499 (Ni + CO in Ar).
(19) Zhou, M. F.; Andrews, L. *J. Am. Chem. Soc.* **1998**, *120*, 13230 (Sc + CO_2).
(20) Frisch, M. J.; Trucks, G. W.; Schlegel, H. B.; Scuseria, G. E.; Robb, M. A.; Cheeseman, J. R.; Zakrzewski, V. G.; Montgomery, J. A., Jr.; Stratmann, R. E.; Burant, J. C.; Dapprich, S.; Millam, J. M.; Daniels, A. D.; Kudin, K. N.; Strain, M. C.; Farkas, O.; Tomasi, J.; Barone, V.; Cossi, M.; Cammi, R.; Mennucci, B.; Pomelli, C.; Adamo, C.; Clifford, S.; Ochterski, J.; Petersson, G. A.; Ayala, P. Y.; Cui, Q.; Morokuma, K.; Malick, D. K.; Rabuck, A. D.; Raghavachari, K.; Foresman, J. B.; Cioslowski, J.; Ortiz, J. V.; Stefanov, B. B.; Liu, G.; Liashenko, A.; Piskorz, P.; Komaromi, I.; Gomperts, R.; Martin, R. L.; Fox, D. J.; Keith, T.; Al-Laham, M. A.; Peng, C. Y.; Nanayakkara, A.; Gonzalez, C.; Challacombe, M.; Gill, P. M. W.; Johnson, B. G.; Chen, W.; Wong, M. W.; Andres, J. L.; Head-Gordon, M.; Replogle, E. S.; Pople, J. A. *Gaussian 98*, revision A.7; Gaussian, Inc.: Pittsburgh, PA, 1998.
(21) Becke, A. D. *Phys. Rev. A* **1988**, *38*, 3098.
(22) Perdew, J. P.; Wang, Y. *Phys. Rev. B* **1992**, *45*, 13 244.
(23) Becke, A. D. *J. Chem. Phys.* **1993**, *98*, 5648.
(24) Krishnan, R.; Binkley, J. S.; Seeger, R.; Pople, J. A. *J. Chem. Phys.* **1980**, *72*, 650.
(25) McLean, A. D.; Chandler, G. S. *J. Chem. Phys.* **1980**, *72*, 5639; Krishnan, R.; Binkley, J. S.; Seeger, R.; Pople, J. A. *J. Chem. Phys.* **1980**, *72*, 650.
(26) Wachters, H. J. H. *J. Chem. Phys.* **1970**, *52*, 1033; Hay, P. J. *J. Chem. Phys.* **1977**, *66*, 4377.
(27) Andrews, L.; Zhou, M. F.; Willson, S. P.; Kushto, G. P.; Snis, A.; Panas, I. *J. Chem. Phys.* **1998**, *109*, 177 (argon), and references therein.
(28) Andrews, L.; Zhou, M. F. *J. Chem. Phys.* **1999**, *111*, 6036 (neon), and references therein.
(29) Lugez, C. L.; Thompson, W. E.; Jacox, M. E.; Snis, A.; Panis, I. *J. Chem. Phys.* **1999**, *110*, 10 345 (neon), and references therein.
(30) Chertihin, G. V.; Andrews, L.; Rosi, M.; Bauschlicher, C. W., Jr. *J. Phys. Chem. A* **1997**, *101*, 9085.
(31) Chertihin, G. V.; Andrews, L. *J. Phys. Chem.* **1995**, *99*, 6356, and references therein.
(32) Andrews, L.; Liang, B. *J. Am. Chem. Soc.* **2001**, *123*, 1997.
(33) Thomas, J. L. C.; Bauschlicher, C. W., Jr.; Hall, M. B. *J. Phys. Chem.* A **1997**, *101*, 8530.
(34) Kushto, G. P.; Andrews, L. *J. Phys. Chem. A* **1999**, *103*, 4836.
(35) Bauschlicher, C. W., Jr.; Siegbahn, P. E. M. *J. Chem. Phys.* **1986**, *85*, 2802.
(36) Williamson, R. L.; Hall, M. B. *Int. J. Quantum Chem. Quantum Chem. Symp.* **1987**, *21*, 503.
(37) Smith, S.; Hillier, I. H.; Von Niessen, W.; Guest, M. F. *Chem. Phys.* **1989**, *135*, 357.
(38) Fronzoni, G.; Decleva, P.; Lisini, A. *Chem. Phys.* **1993**, *174*, 57.
(39) Pedocchi, L.; Rovida, G.; Russo, N. *J. Electron. Spectrosc. Relat. Phenom.* **1994**, *69*, 81.
(40) Bohr, F.; Chermette, H.; Ruiz-Lopez, M. F. *Int. J. Quantum Chem.* **1994**, *52*, 1039.
(41) Andrews, L.; Citra, A. *Chem. Rev.* **2002**, in press.
(42) Jacox, M. E. *Chem. Phys.* **1994**, *189*, 149.
(43) Swanson, B. I.; Satija, S. K. *J. C. S. Chem. Commun.* **1973**, 40.
(44) Hedberg, L.; Hedberg, K.; Satija, S. K.; Swanson, B. I. *Inorg. Chem.* **1985**, *24*, 2766.
(45) A new $^3A'$ state was located 0.5 kcal/mol higher in energy with μ = 5.79 D, but the frequencies (878.9 cm^{-1} (132 km/mol), 536.3 cm^{-1} (37 km/mol), 142.6 cm^{-1} (37 km/mol) do not fit the observed spectra as well as the $^3A''$ state frequencies.